Supplementary Material

Multifaceted Classification and Integration of Time-Varying Complex Signals using Analog Neuromorphic UV Phototransistors

Mohit Kumar,[a,b,*] Suwan Lee,[b] Hyunmin Dang,[b] and Hyungtak Seo[a,b,*]

[a]Department of Energy Systems Research, Ajou University, Suwon, 16499, Republic of Korea,

[b]Department of Materials Science and Engineering, Ajou University, Suwon, 16499, Republic of Korea,

Email: mohitiopb@ajou.ac.kr (M.K.), hseo@ajou.ac.kr (H.S.)

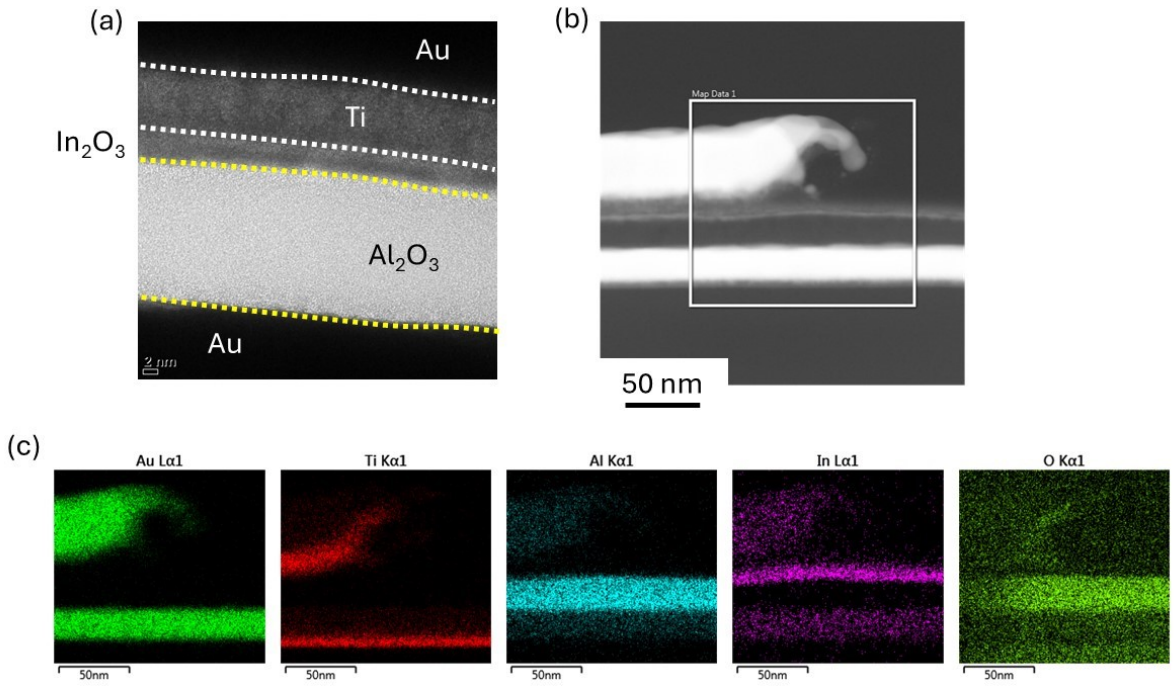

Fig. S1. Cross-sectional analysis of a multilayered structure composed of Au, Ti, Al_2O_3, and In_2O_3 layers. (a) High-resolution transmission electron microscopy (HRTEM) image showing the distinct layers within the structure. The layers include gold (Au) at the top and bottom, titanium (Ti) and aluminum oxide (Al_2O_3) in the middle, and indium oxide (In_2O_3) at the uppermost layer. The boundaries between these layers are indicated by dotted lines: white dots for Au/Ti and Ti/In_2O_3 interfaces, and yellow dots for the Au/Al_2O_3 interface. The scale bar represents 2 nm. (b) TEM image providing a broader view of the multilayered structure. The highlighted square marks the area subjected to elemental mapping. The scale bar indicates 50 nm. (c) Energy-dispersive X-ray spectroscopy (EDS) elemental maps of the highlighted region in (b). These maps show the distribution of the following elements: Gold (Au, Lα1): Green signal showing the distribution of gold. Titanium (Ti, Kα1): Red signal indicating the distribution of titanium. Aluminum (Al, Kα1): Cyan signal representing the distribution of aluminum within the Al_2O_3 layer. Indium (In, Lα1): Magenta signal showing the distribution of indium within the In_2O_3 layer. Oxygen (O, Kα1): Green signal indicating the distribution of oxygen, particularly in the oxide layers (Al_2O_3 and In_2O_3).

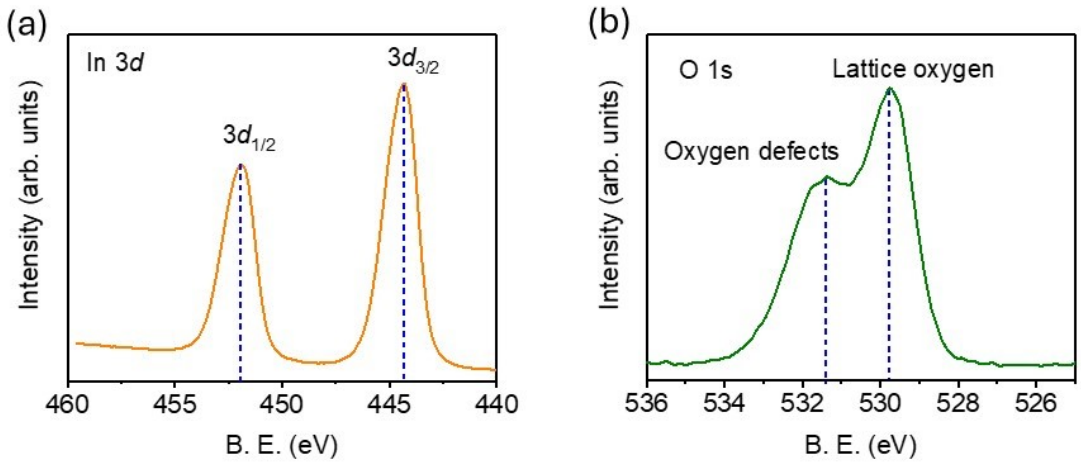

Fig. S2. X-ray photoelectron spectroscopy (XPS) spectra of the In_2O_3 thin film showing the binding energy (B.E.) and corresponding peaks for indium (In) and oxygen (O). (a) XPS spectrum of indium (In 3d) displaying two distinct peaks. The peaks correspond to the spin-orbit split components of indium: In $3d_{5/2}$ at a binding energy of approximately 444.5 eV and In $3d_{3/2}$ at approximately 451.0 eV. The blue dashed lines indicate the positions of these peaks. (b) XPS spectrum of oxygen (O 1s) showing the presence of two main features. The peak at approximately 530.5 eV corresponds to lattice oxygen in the In_2O_3 structure, while the shoulder at around 532.0 eV is attributed to oxygen defects or hydroxyl groups. The blue dashed lines mark the positions of these features.

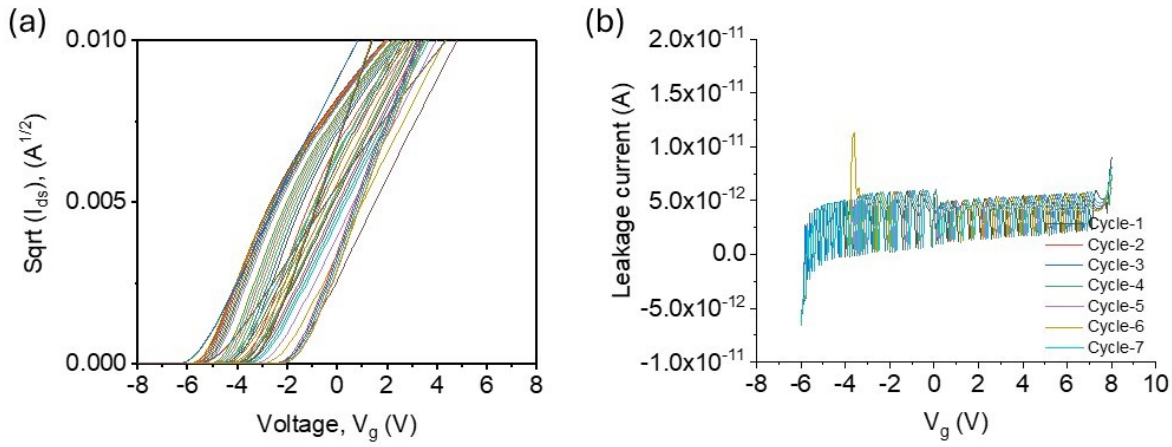

Fig. S3. Electrical characterization of the In_2O_3 thin film transistor (TFT) over multiple cycles, showing transfer characteristics and leakage current behavior. (a) Plot of the square root of the drain current (I_{ds}) versus gate voltage (V_g). (b) Leakage current (I_{leak}) versus gate voltage (V_g) for the TFT measured over seven cycles. The graph displays the low leakage current (~10^{-12} A) behavior, highlighting the stability and reliability of the device under repeated cycling.

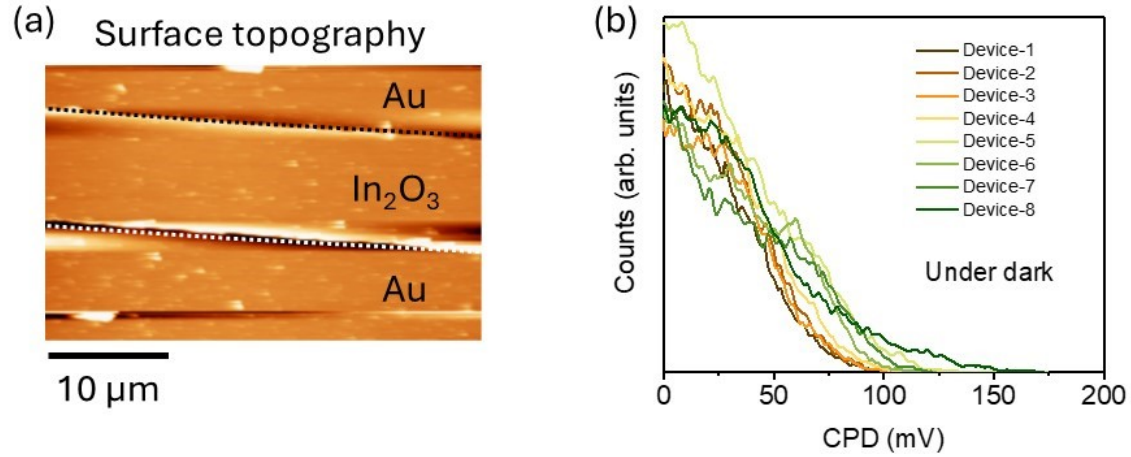

Fig. S4. Surface topography and contact potential difference (CPD) measurements of the Au/In_2O_3/Au structure under dark conditions. (a) Atomic force microscopy (AFM) image showing the surface topography of the structure comprising gold (Au) and indium oxide (In_2O_3). The image highlights the clear distinction between the Au and In_2O_3 layers, marked by dotted lines. The scale bar represents 10 µm. (b) Contact potential difference (V_{cpd}) measurements for multiple devices (Device-1 to Device-8) under dark conditions. Each curve corresponds to a different device, demonstrating the variation in V_{cpd} among the devices. The consistent shape and overlap of the curves suggest similar surface properties and electronic behavior across the devices.

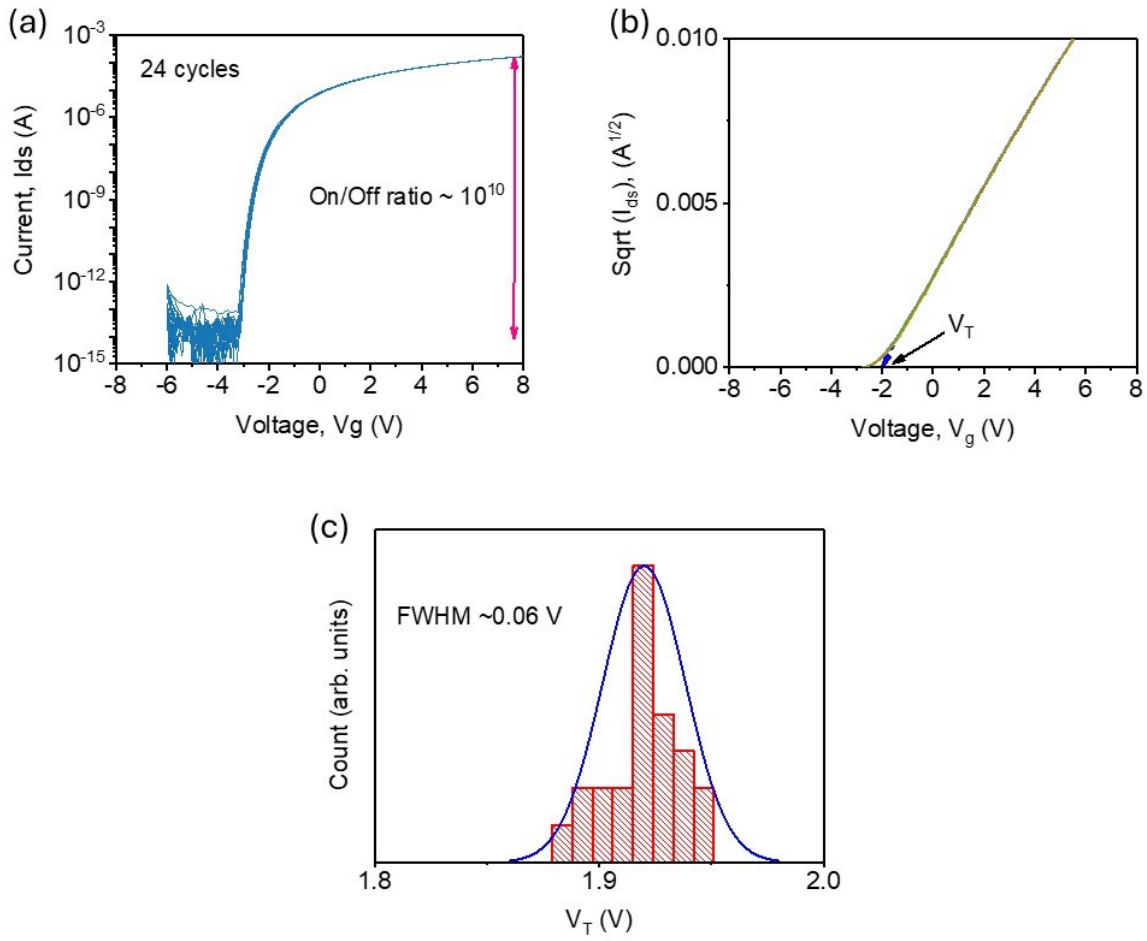

Fig. S5. Electrical performance and threshold voltage (V_T) distribution of the In_2O_3 thin film transistor (TFT) over multiple cycles. (a) Transfer characteristic of the In_2O_3 TFT measured over 24 cycles. The graph shows the drain current (I_{ds}) as a function of gate voltage (V_g), with a demonstrated on/off current ratio of approximately 10^{10}. The high on/off ratio and the consistency over multiple cycles underscore the device's robust switching performance. (b) Plot of the square root of the drain current (I_{ds}) versus gate voltage (V_g). The linear region of the plot is used to extract the V_T, indicated by the arrow. (c) Histogram of the V_T distribution for the In_2O_3 TFT. The histogram is based on measurements from multiple cycles, showing a mean V_T around 1.9 V with a full width at half maximum (FWHM) of approximately 0.06 V.

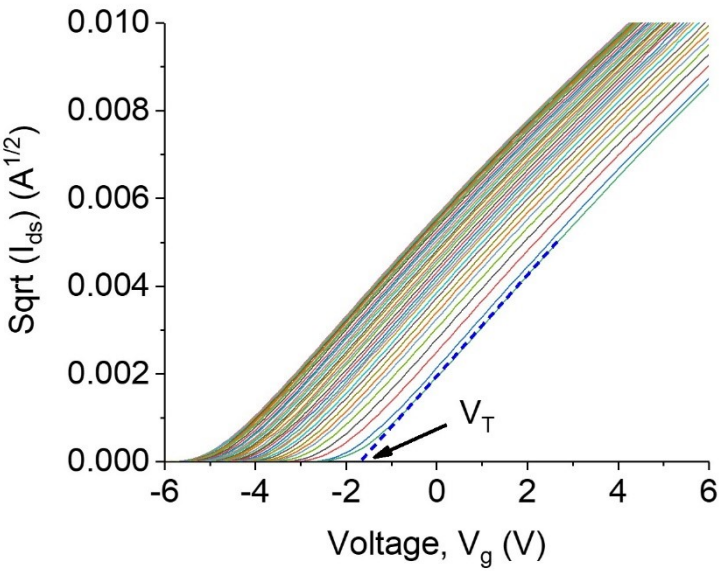

Fig. S6. Threshold voltage (V_T) extraction from transfer characteristics of In_2O_3 thin film transistors (TFTs). The plot shows the square root of the drain current (I_{ds}) versus gate voltage (V_g) with illumination time.

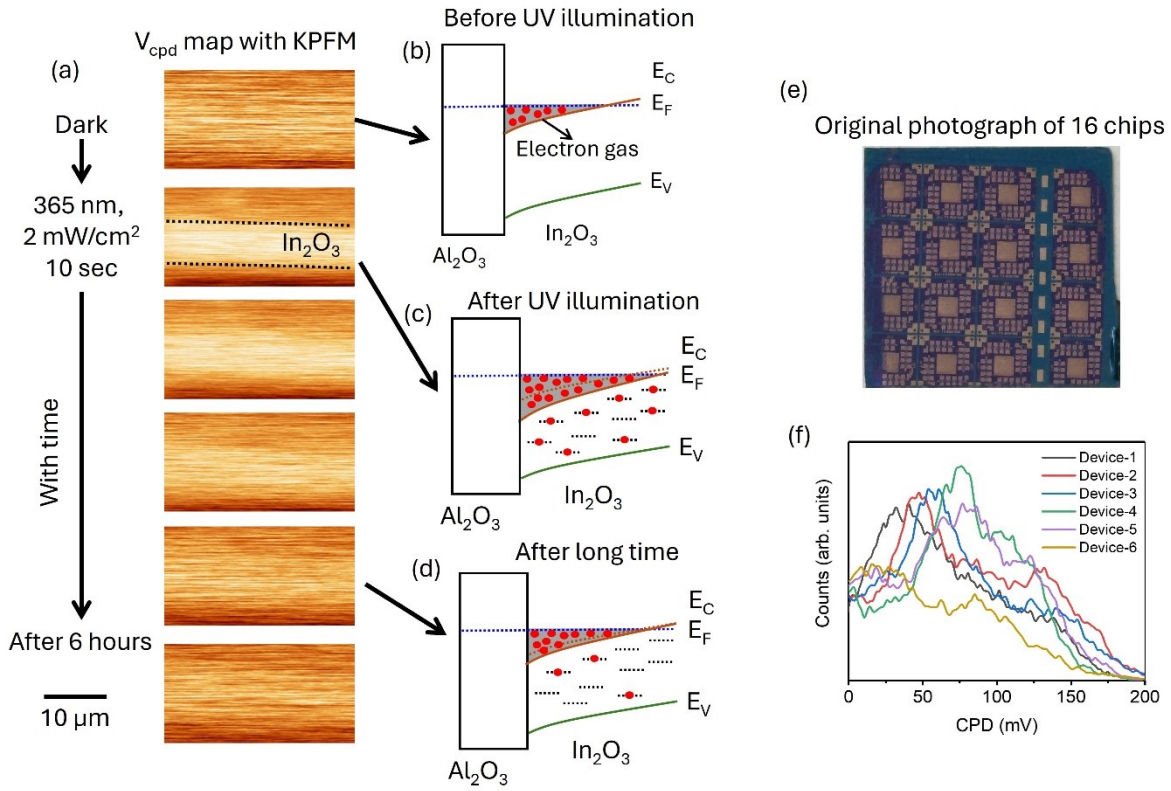

Fig. S7. Schematic diagram illustrating the working mechanism of the neuromorphic optical sensor and the role of persistent photoconductivity, charge trapping, and detrapping in dynamic memory and UV signal classification. (a) Contact potential difference (V_{cpd}) map acquired through Kelvin Probe Force Microscopy (KPFM) under different conditions: initially in the dark, then under UV illumination (365 nm, 2 mW/cm^2, 10 seconds), and over time up to 6 hours post-illumination. This V_{cpd} map demonstrates the gradual recovery of surface potential after UV exposure, indicating persistent photoconductivity and the effects of charge trapping and detrapping. Scale bar = 10 µm. (b) Energy band diagram before UV illumination, showing the Al_2O_3/In_2O_3 interface with a two-dimensional electron gas (2DEG) near the conduction band (E_C) level in the In_2O_3 layer. (c) Energy band diagram immediately after UV illumination, depicting the increased electron density in the 2DEG region due to UV-induced charge trapping near the interface, which shifts the Fermi level (E_F) upward and enhances conductivity. (d) Energy band diagram showing the gradual detrapping of charges over time, as electrons slowly escape from traps, leading to a gradual decrease in the electron density in the 2DEG and a reduction in photocurrent. This slow detrapping process underpins the dynamic memory effect, allowing for the classification of UV signals based on the persistence and decay of the photocurrent. (e) Photograph of a full-length device containing 16 In_2O_3 chips used for the experiments. This image shows the arrangement and layout of the devices on the chip. (f) V_{cpd} measurements for multiple devices (Device-1 to Device-6) after illuminating with UV (365 nm, 2 mW-cm^{-2}, 10 seconds), indicating the variation in surface potential among the devices. The measurements demonstrate the distribution of CPD values, which is crucial for understanding the electronic properties of the devices.

V_T variation of total 56 device devices

3.17	5.34	4.57	3.68	3.33
3.02	5.21	3.97	4.2	4.22
3.08	4.96	5.15	3.41	5.25
2.92	5.56	5.26	4.34	4.26
2.67	6.04	3.39	3.66	3.46
1.6	3.21	5.23	5.19	5.29
1.68	3.25	5.17	1.99	3.72
1.7	3.39	3.83	3.6	5.92
1.93	3.15	4.1	4.1	5.46
1.86	3.29	5.58	3.66	4.26
2.28	4.65	5.38	4.59	

Selected devices

Fig. S8. Variation of threshold voltage (V_T) across 56 In_2O_3 thin film transistor devices. The table displays the V_T values in volts for each device, with selected devices highlighted by a red outline.

Dark condition

3.17	5.34	4.57	3.68	3.33
3.02	5.21	3.97	4.2	4.22
3.08	4.96	5.15	3.41	5.25
2.92	5.56	5.26	4.34	4.26
2.67	6.04	3.39	3.66	3.46

	10 sec					60 sec					180 sec				
310 nm	3.20	5.48	4.80	3.80	3.39	3.52	6.00	5.33	4.27	3.66	4.19	7.10	6.26	5.01	4.53
	3.17	5.38	4.08	4.43	4.46	3.58	5.99	4.54	5.00	5.01	4.17	7.06	5.32	5.84	5.90
	3.16	5.05	5.26	3.60	5.45	3.49	5.45	5.76	4.09	6.04	4.11	6.40	6.78	4.71	7.04
	3.06	5.67	5.57	4.54	4.43	3.42	6.13	6.31	5.07	4.95	4.01	7.23	7.36	5.81	5.58
	2.81	6.31	3.48	3.79	3.61	3.18	7.12	3.83	4.21	4.10	3.70	8.24	4.49	4.94	4.72
365 nm	3.20	5.41	4.74	3.76	3.36	3.36	5.69	5.03	4.05	3.62	3.80	6.50	5.80	4.61	4.24
	3.12	5.34	4.04	4.35	4.38	3.35	5.68	4.31	4.69	4.70	3.90	6.46	4.91	5.44	5.48
	3.12	5.06	5.21	3.54	5.38	3.30	5.24	5.52	3.81	5.73	3.73	5.88	6.17	4.42	6.47
	3.02	5.62	5.46	4.47	4.37	3.24	5.89	5.88	4.78	4.70	3.74	6.63	6.84	5.41	5.06
	2.77	6.26	3.45	3.76	3.57	2.99	6.71	3.66	4.00	3.86	3.44	7.57	4.14	4.59	4.35
395 nm	3.18	5.38	4.64	3.72	3.35	3.26	5.51	4.78	3.84	3.47	3.44	5.80	5.10	4.06	3.71
	3.06	5.28	4.01	4.27	4.30	3.18	5.44	4.13	4.43	4.45	3.37	5.73	4.33	4.69	4.73
	3.10	5.01	5.20	3.46	5.31	3.21	5.11	5.32	3.61	5.48	3.36	5.36	5.57	3.82	5.75
	2.97	5.56	5.35	4.40	4.32	3.06	5.73	5.56	4.54	4.48	3.25	6.07	5.90	4.78	4.60
	2.70	6.16	3.42	3.70	3.50	2.83	6.37	3.51	3.82	3.66	3.00	6.65	3.70	4.05	3.82

Fig. S9. Threshold voltage (V_T) variation in In_2O_3 thin film transistors under different UV exposure conditions. The tables show the V_T values in volts for devices measured in dark conditions and after exposure to UV light at wavelengths of 310 nm, 365 nm, and 395 nm for durations of 10 seconds, 60 seconds, and 180 seconds. The data highlights the impact of UV exposure on the V_T values across multiple devices, demonstrating the dependency on wavelength and exposure time. This data corresponds to the matrix in Figure 2j in main text.

Dark condition

3.17	5.34	4.57	3.68	3.33
3.02	5.21	3.97	4.2	4.22
3.08	4.96	5.15	3.41	5.25
2.92	5.56	5.26	4.34	4.26
2.67	6.04	3.39	3.66	3.46

		10 sec					60 sec					180 sec				
310 nm		3.18	5.44	4.76	3.77	3.36	3.48	5.91	5.24	4.19	3.61	4.14	6.95	6.14	4.90	4.45
		3.15	5.34	4.05	4.39	4.43	3.51	5.91	4.47	4.92	4.93	4.12	6.93	5.24	5.76	5.78
		3.13	5.01	5.23	3.58	5.42	3.42	5.39	5.67	4.02	5.93	4.03	6.31	6.69	4.63	6.92
		3.03	5.63	5.54	4.50	4.39	3.36	6.03	6.20	5.00	4.86	3.95	7.12	7.26	5.72	5.46
		2.79	6.26	3.45	3.76	3.58	3.12	7.03	3.75	4.15	4.05	3.64	8.08	4.40	4.83	4.65
After 60 mins	365 nm	3.18	5.37	4.72	3.73	3.33	3.31	5.58	4.96	3.97	3.56	3.75	6.38	5.67	4.51	4.17
		3.10	5.30	4.01	4.31	4.35	3.29	5.61	4.22	4.60	4.61	3.82	6.36	4.83	5.35	5.38
		3.09	5.01	5.18	3.52	5.35	3.24	5.15	5.45	3.76	5.62	3.68	5.79	6.09	4.34	6.34
		3.00	5.59	5.44	4.43	4.33	3.19	5.77	5.78	4.72	4.63	3.68	6.55	6.73	5.31	5.00
		2.75	6.22	3.42	3.74	3.54	2.93	6.56	3.59	3.92	3.81	3.39	7.46	4.07	4.50	4.30
After 60 mins	395 nm	3.16	5.34	4.62	3.68	3.33	3.21	5.39	4.72	3.79	3.42	3.40	5.73	5.04	4.00	3.64
		3.04	5.24	3.99	4.24	4.28	3.12	5.34	4.06	4.35	4.38	3.32	5.63	4.25	4.62	4.65
		3.08	4.97	5.17	3.44	5.28	3.16	5.00	5.25	3.53	5.38	3.30	5.24	5.45	3.74	5.64
		2.95	5.52	5.32	4.36	4.30	3.01	5.62	5.46	4.46	4.43	3.19	5.97	5.82	4.70	4.56
		2.68	6.11	3.39	3.68	3.47	2.78	6.27	3.46	3.77	3.60	2.94	6.54	3.65	4.00	3.74

Fig. S10. Threshold voltage (V_T) variation in In_2O_3 thin film transistors under dark conditions and after UV exposure followed by a 60-minute recovery period. The tables display the V_T values in volts for devices measured in dark conditions and after exposure to UV light at wavelengths of 310 nm, 365 nm, and 395 nm for 10 seconds, 60 seconds, and 180 seconds. The second set of tables shows the V_T values after a 60-minute recovery period post-exposure. This data illustrates the impact of UV exposure and subsequent recovery on the V_T values across multiple devices, demonstrating the effects of different wavelengths and exposure durations.

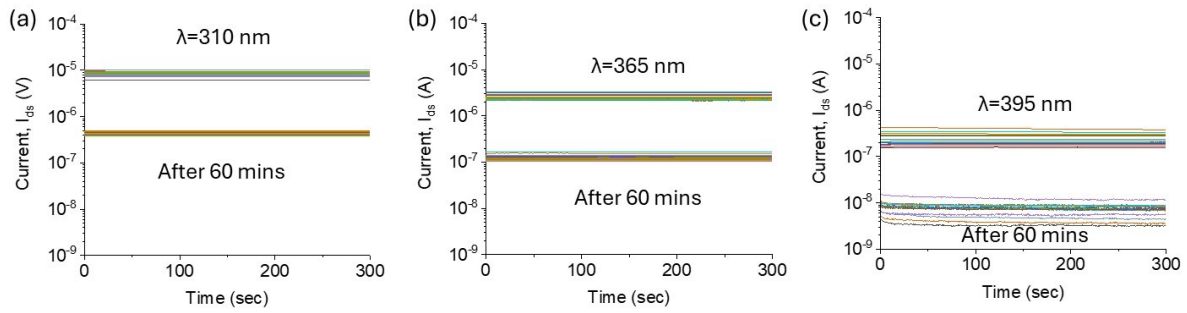

Fig. S11. Drain current (I_{ds}) variation in In_2O_3 thin film transistors under continuous UV exposure and after a 60-minute recovery period. (a) under UV exposure at 310 nm for 300 seconds and the current measured after a 60-minute recovery period. (b) I_{ds} versus time under UV exposure at 365 nm for 300 seconds and the current measured after a 60-minute recovery period. (c) I_{ds} versus time under UV exposure at 395 nm for 300 seconds and the current measured after a 60-minute recovery period.

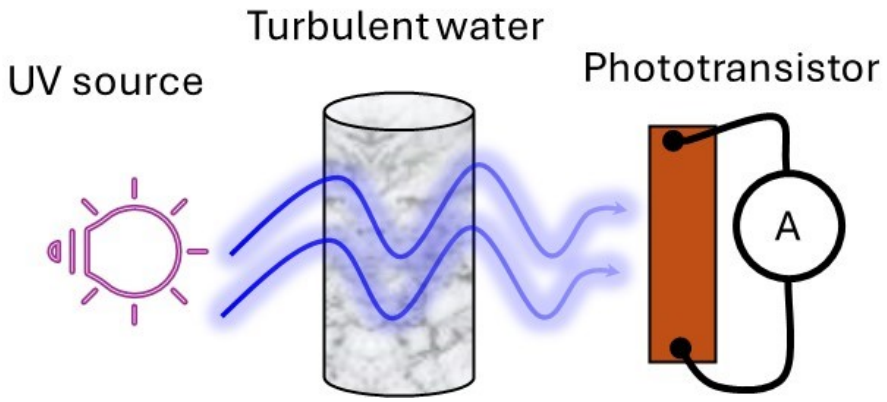

Fig. S12. Schematic diagram of the experimental setup used to measure the effect of UV light on a phototransistor through turbulent water. The setup includes a UV light source, turbulent water as the medium, and a phototransistor connected to source meter for current measurement. The UV light passes through the turbulent water, which may scatter and attenuate the light before it reaches the phototransistor. This configuration is used to study the impact of water-induced turbulence on the performance of the phototransistor under UV illumination.